LAWRENCE
LIVERMORE
NATIONAL
LABORATORY

UCRL-CONF-208356

The Electrochemical Behavior of Alloy 22 in Extreme Chloride and Nitrate Environments

R. A. Etien, S. R. Gordon, G. O. Ilevbare

December 2, 2004

NACE International, CORROSION/2005
Houston, TX, United States
April 3, 2005 through April 7, 2005

THE ELECTROCHEMICAL BEHAVIOR OF ALLOY 22 IN EXTREME CHLORIDE AND NITRATE ENVIRONMENTS

R.A. Etien, S.R. Gordon and G.O. Ilevbare

Lawrence Livermore National Laboratory, Livermore, CA 94550, USA

ABSTRACT

Alloy 22 specimens were tested in high temperature, high concentration chloride and nitrate environments. Results of this study indicate that increasing nitrate to chloride ratio in these electrolytes increases resistance to localized breakdown and mitigates repassivation. Open circuit (E_{corr}), breakdown and repassivation potentials all increase, and localized corrosion morphology changes as nitrate to chloride ratio increases. Results also indicate that increasing the temperature increases E_{corr} values, while breakdown potentials and repassivation potentials peak at 130^{o}C for the highest nitrate to chloride ratio electrolytes.

Keywords: Alloy 22, localized corrosion, nitrate, chloride, welds, deliquescence

INTRODUCTION

Alloy 22 is a nickel based alloy that is highly corrosion resistant. It falls into the general category of nickel-chromium-molybdenum alloys known for their high corrosion resistance. Like other alloys in this family, Alloy 22 exhibits both low general corrosion rates and high resistance to localized corrosion in a wide range of environments.[1-8]

Alloy 22 is the material to be used for the waste packages for the underground storage of radioactive waste at Yucca Mountain. One of the most probable exposure mechanisms of the waste packages to aqueous solutions will be through the process of deliquescence. Deliquescence is the process by which a crystalline solid absorbs moisture and subsequently dissolves. As the waste packages cool and the relative humidity rises, the likelihood of deliquescence occurring on the package surface increases. The initial solutions that form through this process are predicted to exist at high temperatures (probably above 100^{o}C) and contain high salt concentrations.[9, 10]

Solutions containing high amounts of chloride and nitrate have been identified as one type of deliquescence solution that is likely to form in the repository.[10] Nitrate has been shown to have an inhibitive effect on the localized corrosion behavior of Alloy 22 in chloride solutions at lower

concentrations and temperatures than those expected in a deliquescence solution.[2, 3, 7] Dunn and Brossia found that for welded Alloy 22 specimens tested in 0.5 M NaCl solutions at 95°C, there was no crevice corrosion initiated in potentiodynamic tests for nitrate to chloride ratios of 0.2 or greater but crevice corrosion did occur at ratios of 0.1 and below.[3] Evans et. al. found that in potentiodynamic testing of Alloy 22 in 5 M calcium chloride ($CaCl_2$) solutions, the onset of localized corrosion could be shifted from 75°C to 105°C by adding 0.5 M calcium nitrate ($Ca(NO_3)_2$).[2] As the ratio of nitrate to chloride is increased, an increase in both breakdown potentials and repassivation potentials occurs, and the difference between these potentials and open circuit values increases.[2, 3, 7] In this study the effect of nitrate on localized corrosion of welded Alloy 22 specimens at extremes of chloride concentration and temperature in $CaCl_2$ + $Ca(NO_3)_2$ solutions was examined.

EXPERIMENTAL

Alloy 22 specimens were prepared from welded plate specimens. The welds were made by means of Gas Tungsten Arc Welding (GTAW). These specimens were set up in a multiple crevice assembly (MCA) based on crevice formers described in ASTM G 48, (Figure 1).[11] In addition to the Alloy 22 specimen, the MCA set-ups consisted of ceramic crevice formers and titanium grade 2 bolts, nuts and washers. A layer of polytetrafluoroethylene (PTFE) tape was inserted between the crevice formers and the specimens in order to fill any microvoids and create reproducibly tight crevices. The surface of the titanium bolt was insulated from the specimen using polyolefin shrink fit tubing.

The working surfaces on the MCA specimens were polished to a 600 grit finish using SiC paper. The areas perpendicular to the surface on which the crevice former rested (edge of specimen) were sequentially polished using 100, 240 and 600 grit papers in order to remove damage done by electric discharge machining (EDM) during fabrication of the specimens by the supplier. After polishing, the specimens were sequentially degreased using hexane, acetone and methanol. After degreasing the specimens were assembled.

Electrochemical testing was conducted using a three electrode setup with a saturated silver/silver chloride (SSC) reference electrode and a platinum counter electrode measuring roughly 40 cm^2 in surface area. The reference electrode was cooled using a cooling jacket with flowing water maintained at 5 to 12°C. A water cooled condenser was also used to minimize evaporative concentrating of solutions. Solutions were deaerated using nitrogen gas flowing at a rate of 50 to 100 cc per minute. Nitrogen escaping from the condenser outlet was bubbled through water in order to avoid any backflow of oxygen from the air.

For each specimen tested, three different electrochemical tests were conducted. First, a twenty-four hour monitoring of the open circuit potential (E_{corr}) was done. Immediately following this, a series of polarization resistance tests were performed from which passive corrosion rates were calculated. For the passive corrosion rate calculations, tafel slopes of 0.12 V per decade and equivalent weights of 23.28 were assumed. Finally a cyclic potentiodynamic polarization (CP) test was performed. The CP scans started at approximately 100 mV below the corrosion potential (E_{corr}) and continued until a current density of 5 $mAcm^{-2}$ or a maximum voltage reading of up to 1 V (SSC) was reached before the scan was reversed. The scan rate used for the forward and reverse sweeps was 0.1667 mVs^{-1}.

Nine different solutions under eleven different conditions were used for testing. These are tabulated in Table 1. Three different $CaCl_2$ compositions were chosen. For each $CaCl_2$ composition, $Ca(NO_3)_2$ was added in order to generate a nitrate to chloride ratio (NO_3^-:Cl^- ratio) of 0.05, 0.15, or 0.5. It was necessary to use three different $CaCl_2$ concentrations, in order to cover the desired temperature range of

100 to 160°C. The 160°C solutions are solid at 100°C, and the 100 and 130°C solutions boil at 160°C. The 12 molal $CaCl_2$ + 6 molal $Ca(NO_3)_2$ solution was used at three different test temperatures to investigate the effect of temperature on the measured parameters. All chemicals used to prepare the electrolytes were of ACS reagent grade.

Cyclic polarization data was analyzed for breakdown potential (E_{20}) and for repassivation potential (E_{r1}). E_{20} is the potential where current density first reaches 2e-5 Acm^{-2} (20 μAcm^{-2}) on the forward anodic scan of the polarization curve. It is a measure of resistance to initiation of localized corrosion. E_{r1} is the potential where a decaying current density reaches 1e-6 Acm^{-2} (1 μAcm^{-2}) on the reverse scan of the polarization curve, that is, below the chosen potential, the current density consistently remains below a current density of 1 μAcm^{-2} in the anodic portion of the reverse scan. The repassivation potential E_{r1} is a measure of how easily a specimen repassivates once localized corrosion has initiated, and represents the potential below which self sustaining localized corrosion is not expected to occur.

RESULTS

Figure 2 shows 24 hour E_{corr} values plotted against temperature (bottom x-axis) and $CaCl_2$ concentration (top x-axis) for the different NO_3^-:Cl^- ratios. The lines shown in the plots are interpolation lines used as aids to show trends in the data. They have no other physical meaning. It can be seen that the 0.5 NO_3^-:Cl^- ratio solutions show more noble E_{corr} values compared with 0.05 and 0.15 ratio solutions at constant temperature and chloride concentration ($[Cl^-]$) in the 130 and 160°C electrolytes (moving vertically). For the 100°C electrolytes, this trend is not apparent due to large scatter in the E_{corr} values for the 0.15 NO_3^-:Cl^- ratio electrolyte. The E_{corr} values also show a tendency to increase with electrolyte concentration ($[Cl^-]$ and $[NO_3^-]$) and temperature (moving horizontally). Note that the $CaCl_2$ concentrations shown in Figure 2 (and subsequent figures) are not plotted to scale, but are used to delineate the data points with their corresponding $CaCl_2$ concentrations. Thus, increasing temperatures also correspond to increasing Cl^- and NO_3^- (solute) concentrations.

Figure 3 shows corrosion rate data plotted against temperature and $CaCl_2$ concentration for the different NO_3^-:Cl^- ratios. The data shows that passive corrosion rate falls as the NO_3^-:Cl^- ratio increases for a given temperature and $[Cl^-]$. The passive corrosion rate does not appear to show a strong response to increasing $[Cl^-]$ (within a fixed NO_3^-:Cl^- ratio) and temperature, suggesting that the NO_3^-:Cl^- ratio is a stronger influencing factor on passive corrosion rates (near E_{corr}) for Alloy 22 than absolute $[Cl^-]$ or temperature in these electrolytes.

Figures 4 and 5 show examples of polarization curves taken in these extreme environments. Figure 4 is a polarization curve for a specimen tested in 10 molal $CaCl_2$ + 5 molal $Ca(NO_3)_2$ at 100°C. The curve exhibits a large intermediate peak on the forward scan that reaches a maximum near 0.4 V. E_{20} is reached at 0.208 V on the forward scan. A further increase in potential results in the stepwise drop of the current density of the specimen until repassivation occurs at about 750 mV. A further increase in the potential results in another increase in current, this time due to transpassive dissolution. This was confirmed by visual inspection of the specimen, and by the fact that a reversal of the potential at 1 V does not result in a hysteresis loop, which would have been indicative of localized breakdown. The curve also shows some unconventional behavior on its reverse scan. The current density immediately begins to drop when the current scan is reversed at 1 V. The current density drops below 1 μAcm^{-2} at 0.691 V. This trend continues until the reverse scan changes to cathodic behavior for a very small potential range (0.525 to 0.490 V), implying the reduction of an oxidized specie (oxidized during the forward scan). At roughly 0.490 V, the current density once again switches back to anodic behavior and the current density increases to values above 1 μAcm^{-2} and reaches a peak of 60 μAcm^{-2} near 0.25 V

before decreasing below 1 μAcm^{-2} once again at 0.078 V. For a polarization curve showing reactivation behavior like this, the E_{r1} value is the second potential value (lowest value) where current density drops below 1 μAcm^{-2}, in this case 0.078 V.

Figure 5 shows three polarization curves taken for the three different NO_3^-:Cl^- ratios for 12 molal $CaCl_2$ at 130°C. The polarization curves for the 0.05 and 0.15 NO_3^-:Cl^- ratio solutions both exhibit little or no passive behavior and show significant hysteresis behavior on the reverse scan. They both reach their reverse current density criterion of 5 $mAcm^{-2}$ before reaching the reverse potential criteria of 1 V. The scan for the 0.5 NO_3^-:Cl^- ratio solution, however, exhibits a larger passive range and shows a relatively smaller hysteresis loop. It does not reach the reverse current density before reaching 1 V. This series of curves exhibits a trend of increasing breakdown and repassivation potentials with increasing NO_3^-:Cl^- ratio.

Figure 6 shows E_{20} versus temperature and $CaCl_2$ concentration. E_{20} increases as the NO_3^-:Cl^- ratio increases at a given temperature and [Cl^-], across all temperatures and [Cl-] (moving vertically). The data shows there is a large increase in E_{20} at the higher temperatures (130 and 160°C) and higher concentrations (0.5 NO_3^-:Cl^- ratios) compared with the lower 0.05 and 0.15 ratios. In the lowest temperature, lowest concentration electrolytes (100°C and 10 molal $CaCl_2$), there is still a positive effect on the breakdown potentials (increase) from increasing NO_3^-:Cl^- ratios, but it is not as dramatic as the increase in the 130 and 160°C electrolytes. E_{20} values also generally show an increase when moving to higher temperatures and concentrations ([Cl^-] and [NO_3^-]) for constant NO_3^-:Cl^- ratio (moving horizontally) except when moving from 130 to 160°C for 0.5 NO_3^-:Cl^- ratio electrolytes. The increase is especially dramatic when moving from 100 to 130°C in the 0.5 NO_3^-:Cl^- ratio electrolytes.

Figure 7 shows E_{r1} versus temperature and $CaCl_2$ concentration. The data shows similar trends to E_{20} data (Figure 6). Higher NO_3^-:Cl^- ratios, at a constant temperature and [Cl^-], result in higher E_{r1} values for Alloy 22 (moving vertically). For a given NO_3^-:Cl^- ratio, E_{r1} increases as [Cl^-] and [NO_3^-] increase (moving horizontally). More dramatic increases in Er1 take place in the presence of solutions with a 0.5 NO_3^-:Cl^- ratio, and is consistent with observations made in Figure 6 with E_{20} values.

In general, the trends seen with both E_{20} and E_{r1} are similar to those seen for E_{corr} values. They all show the tendency to move toward more noble values as NO_3^-:Cl^- ratio is increased and also as solutions at a constant NO_3^-:Cl^- ratio become more concentrated and are tested at higher temperatures. The effect of [Cl^-] (or absolute concentration) and temperature does not appear to be as strong as the effect of NO_3^-:Cl^- ratio or absolute [NO_3^-] (Figures 2, 6 and 7).

To help determine the separate effects of temperature and solute concentration on the E_{20}, E_{r1} and E_{corr} of Alloy 22 in these extremely concentrated electrolytes, another series of experiments was conducted. For these experiments a constant electrolyte concentration of 12 molal $CaCl_2$ + 6 molal $Ca(NO_3)_2$ was used while the testing temperature was varied between 100 and 150°C. Figure 8 compares the cyclic polarization behavior of specimens tested in the 12 molal $CaCl_2$ + 6 molal $Ca(NO_3)_2$ electrolytes at 100, 130 and 150 °C. The curves at 100 and 130°C curves exhibit intermediate peaks on the forward scan not shown by the 150°C curve. The re-initiation behavior during the reverse scan of the 100°C curve mentioned previously (Figure 4) can also be seen in Figure 8. Figure 9 shows 24-hour E_{corr}, E_{20} and E_{r1} of Alloy 22 as a function of temperature in 12 molal $CaCl_2$ + 6 molal $Ca(NO_3)_2$. 24-hour E_{corr} values show a consistent increase as a function of temperature. Both the E_{20} and E_{r1} values of Alloy 22 in this electrolyte show an increase between 100 and 130°C and then a decrease in values between 130 and 150°C. Thus, maximum resistance to localized corrosion in this electrolyte is shown at 130°C for Alloy 22. This is a parabolic relationship rather than a linear one.

Observations of all specimens tested in this study showed that localized corrosion occurred on all but one specimen that was tested in 0.5 NO_3^-:Cl^- ratio solution at 160°C. The localized corrosion mechanism was pitting. Crevice corrosion was not observed, in spite of the fact that specimens were multiple crevice assemblies (MCA). Total pitted area became smaller and pit aspect ratio (width to depth) became larger (pitting became shallower) as NO_3^-:Cl^- ratio increased. The total pitted area on all specimens tested in 0.5 NO_3^-:Cl^- ratio electrolytes was small relative to other specimens. Among the 0.5 NO_3^-:Cl^- ratio specimens, those tested at 100°C showed the most pitting.

Pitted zones took on a different appearance in weld versus base zones of the specimen. Figure 10 shows a dark field light microscopy image of pitting at a weld/base metal interface. Most of the surface shown in this image is pitted with pitted areas showing up as light gray or gray in color. In the weld zone, pitting preferentially occurred on either dendrites or interdendritic spaces. A determination of which zone is being preferentially attacked is ongoing. In the base metal zone, pitting occurred randomly, without a preferred area of attack. Pitting did not appear to show a preference toward attack of weld or base metal for these cyclically polarized specimens. Dark field is used in Figure 10 to show the features inside the pitted areas, because pits show up as featureless black areas in bright field images.

DISCUSSION

Results of the current study indicate that in high temperature, high concentration $CaCl_2$ + $Ca(NO_3)_2$ bearing electrolytes the NO_3^-:Cl^- ratio has a strong influence on E_{corr}, breakdown potentials, E_{20}, and repassivation potentials, E_{r1}. These results are consistent with those of other researchers studying Alloy 22 behavior in lower concentration, lower temperature chloride bearing environments.[2,3,7] These results therefore imply that the inhibiting ability of nitrate on localized corrosion is maintained at extremes of chloride concentration and temperature provided that critical ratios of NO_3^-:Cl^- are maintained.

24 hour E_{corr} values are higher for 0.5 NO_3^-:Cl^- ratio solutions than for 0.05 or 0.15 NO_3^-:Cl^- ratio solutions tested at 130 and 160°C (Figure 2). Figure 9 shows that the major contributor to the increase in corrosion potential seen in Figure 2 is temperature. The E_{corr} values shown in Figure 9 roughly correspond to the values for the 0.5 NO_3^-:Cl^- ratio curve from Figure 2. This implies that kinetic effects are important in determining the corrosion potential of Alloy 22 in these electrolytes. Reaction kinetics generally increase with temperature. Nonetheless, E_{corr} data coupled with passive corrosion rate results (Figure 3) indicates that in these electrolytes, nitrate helps to maintain a more effective passivation layer on the Alloy 22 surface in these environments.

Breakdown potentials also increase significantly as the NO_3^-:Cl^- ratios increase from 0.05 to 0.5 at test temperatures of 130 and 160°C (Figure 4). This increase is even larger in magnitude than it is for the E_{corr} values and is consistent with the increase in the passive region of Alloy 22 as observed in Figure 5. These results show that the higher corrosion potentials registered on Alloy 22 in the 0.5 NO_3^-:Cl^- ratio electrolytes translate to more resistant oxide films, and thus higher breakdown and repassivation potentials (Figures 2, 6 and 7). Breakdown and repassivation potentials indicate that nitrate effectively raises breakdown and repassivation to higher potentials, and implies that localized corrosion is more difficult to initiate and repassivation is enhanced as nitrate concentration increases in solution. This is particularly evident at higher temperatures and higher [Cl^-]. E_{20} and E_{r1} values are much higher for the 0.5 NO_3^-:Cl^- ratio electrolytes under the 130 and 160°C testing condition shown in Figures 6 and 7.

The parabolic relationship between E_{20} (and E_{r1}) and temperature is unusual (Figure 9). The increase of E_{20} (and E_{r1}) as temperature is increased suggests that temperature increases the breakdown and

repassivation potentials of Alloy 22 instead of reducing it as is usually observed in experiments of this nature. A couple of possibilities exist as to why E_{20} and E_{r1} first increased with temperature before decreasing upon further increase in temperature. It is possible that increases in temperature allowed thicker, more resistant oxide film to form at temperatures within the test duration time due to higher kinetic energy (ionic mobility) in the system at higher temperature. This film could counteract the higher dissolution rates that are often associated with higher temperature electrolytes. The ability to grow thicker (rather than thinner) oxide films with increase in temperature might be explained by increase in activity of ions in the electrolyte with increase in temperature. The consistency of the electrolyte used is thick at 100°C. It solidifies between 80 and 90°C. So it is not unreasonable to expect that the activity of the ions in the electrolyte will increase as temperature is increased. However, after a certain temperature, any improvement due to increased activity diminishes, and further temperature increases result in a reduction of E_{20} and E_{r1}. Thus, while further increases in temperature above 130°C (in this case) may not lead to thinner or less robust oxide films (as E_{corr} increases with temperature, Figure 9), the increased mobility of Cl^- ions in solution and their ability to cause reductions in E_{20} and E_{r1} start to exceed the ability of any improvement in the oxide film to mitigate localized breakdown. However, the effect of temperature on the breakdown potentials of Alloy 22 may be due to more than just a simple case of thickening the oxide film at the higher temperatures. The presence of the large anodic peak on the 100°C in Figure 4 could result from a phase transformation in the passive film (also applies to Figure 8). Such phase transformations may also be facilitated by a change in the activity of the ions in solution. It is likely that one component of the film is being dissolved and replaced by another. This peak is still present on the 130°C curve, but it is not as prominent. The 150°C curve does not display any peak, which suggests that the passive film is not going through the significant changes that are potentially occurring at the lower temperatures. It can be observed that the passive current density of Alloy 22 increases with increase in temperature (Figure 8).

CONCLUSIONS

- The ability of nitrate to inhibit localized corrosion of welded Alloy 22 specimens is maintained in high concentration, high temperature $CaCl_2 + Ca(NO_3)_2$ electrolytes.
- Welded Alloy 22 specimens tested in NO_3^-:Cl^- ratios of 0.5 show higher resistance to localized corrosion than specimens tested at ratios of 0.15 and 0.05. Breakdown and repassivation values as well as E_{corr} increase when NO_3^-:Cl^- ratio is increased to 0.5 from 0.05 or 0.15.
- Increasing the NO_3^-:Cl^- ratio to 0.5 from 0.05 and 0.15 in these electrolytes widens the range of passive behavior.
- In 0.5 NO_3^-:Cl^- ratio solutions with constant electrolyte concentrations, E_{corr} values increase with increasing temperature, while E_{20} and E_{r1} values peak at 130°C.
- Pit morphology changes as nitrate to chloride ratio increases. At low ratios pits tend to be deeper than at high ratios.

ACKNOWLEDGEMENTS

This work was performed under the auspices of the U.S. Department of Energy by the University of California Lawrence Livermore National Laboratory under contract No. W-7405-Eng-48. This work is supported by the Yucca Mountain Project-LLNL, which is part of the Office of Civilian Radioactive Waste Management (OCRWM).

REFERENCES

1. J. C. Farmer, R. D. McCright, G. E. Gdowski, F. Wang, T. S. E. Summers, P. Bedrossian, J. M.

Horn, T. Lian, J. C. Estill, A. Lingenfelter and W. Haalsey, PVP-ASME, 408, 53 (ASME 2000: New York, NY).
2. K. J. Evans, S. D. Day, G. O. Ilevbare, M. T. Whalen, K. J. King, G. A. Hurst, L. L. Wong, J. C. Estill and R. B. Rebak, *Transportation, Storage, and Disposal of Radioactive Materials*, PVP-Vol. 467, p. 55 (2003).
3. D. S. Dunn and C. S. Brossia, paper 02548, CORROSION 2002, NACE International, Houston, TX (2002).
4. N. S. Meck, P. Crook, S. D. Day and R. B. Rebak, Paper 03, CORROSION 2003, NACE International, Houston, TX (2003).
5. L. L. Wong, D. V. Fix, J. C. Estill, R. D. McCright and R. B. Rebak, 26th Symposium on the Scientific Basis for Nuclear Waste Management as held at the 2002 MRS Fall Meeting; Boston, MA, USA, 2-5 Dec. 2002. pp. 735-742. 2003.
6. R. B. Rebak and P. Crook, Paper 00499, CORROSION 2000, NACE International, Houston, TX (2000).
7. B. A. Kehler, G. O. Ilevbare and J. R. Scully, *Corrosion*, 57, pp. 1042-1065; 2001.
8. R. B. Rebak and J. C. Estill, 26th Symposium on the Scientific Basis for Nuclear Waste Management as held at the 2002 MRS Fall Meeting, Boston, MA, USA, 2-5 Dec. 2002. pp. 713-722. 2003.
9. G. E. Gdowski. "W1045 Environment on the Surfaces of the Drip Shield & Waste Package Outer Barrier", LLNL, Report ANL-EBS-MD-000001.
10. J. Farmer, V. Pasupathi, P. Nair, G. Gordon, D. McCright, G. Gdowski, S. Carroll, T. Steinborn, T. Summers, F. Wong, R. Rebak, R. Lian, G. Ilevbare, J. Lee, F. Hua and J. Payer, "Technical Basis Document No. 6: Waste Package and Drip Shield Corrosion", UCRL-LR-155288.
11. American Society for Testing and Materials, Annual Book of ASTM Standards, Vol.03.02, West Conshohocken, PA: ASTM (2001).

FIGURE 1 - Multiple crevice assembly (MCA) showing lollipop specimens with ceramic crevice formers and titanium grade 2 bolt, nut and washers.

TABLE 1
THE TEST ELECTROLYTES

$CaCl_2$ Concentration	$Ca(NO_3)_2$ Concentrations	Temperature
10 molal	0.5 molal, 1.5 molal, 5 molal	100°C
12 molal	0.6 molal, 1.8 molal, 6 molal	130°C
12 molal	6 molal	100, 150°C
18 molal	0.9 molal, 2.7 molal, 9 molal	160°C

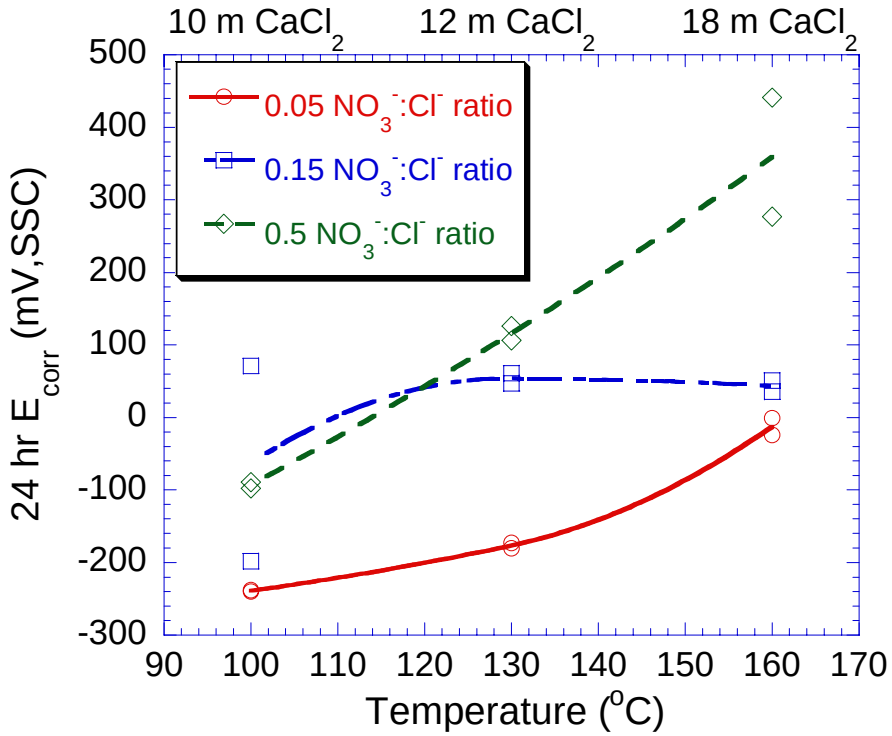

FIGURE 2 - 24 hour E_{corr} values versus temperature (bottom x-axis) and $CaCl_2$ concentration (top x-axis) for 0.05, 0.15 and 0.5 NO_3^-:Cl^- ratios.

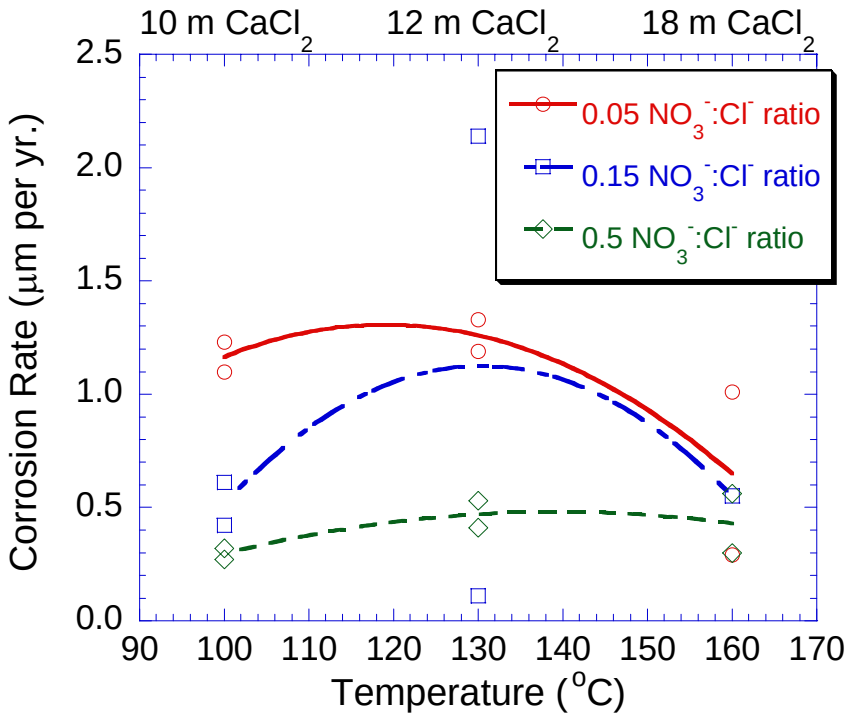

FIGURE 3 - Passive corrosion rate of welded Alloy 22 versus temperature (bottom x-axis) and $CaCl_2$ concentration (top x-axis) for 0.05, 0.15 and 0.5 NO_3^-:Cl^- ratios.

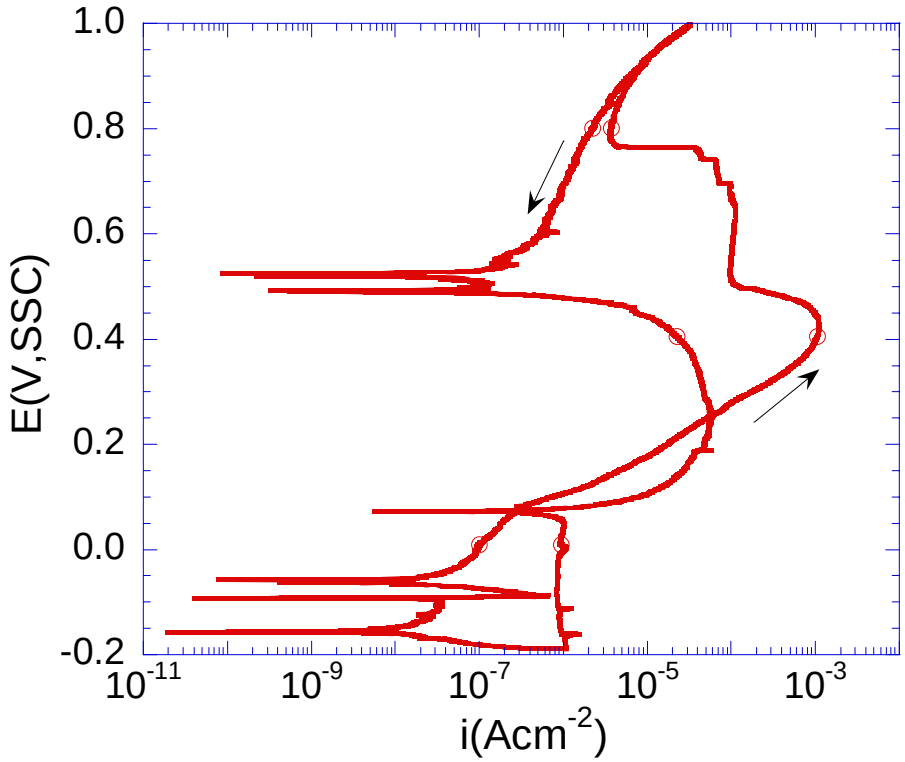

FIGURE 4 - Cyclic polarization curve for specimen tested in 10 molal $CaCl_2$ + 5 molal $Ca(NO_3)_2$ at 100°C.

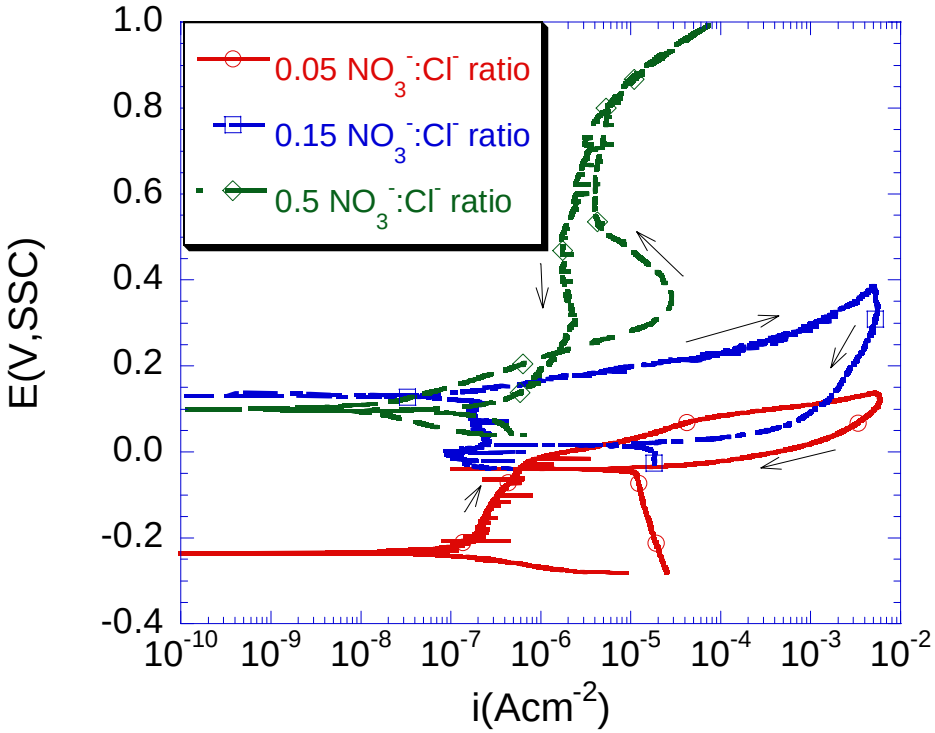

FIGURE 5 - Comparison of polarization curves for 0.05, 0.15 and 0.5 NO_3^-:Cl^- ratios containing 12 molal $CaCl_2$ at 130°C.

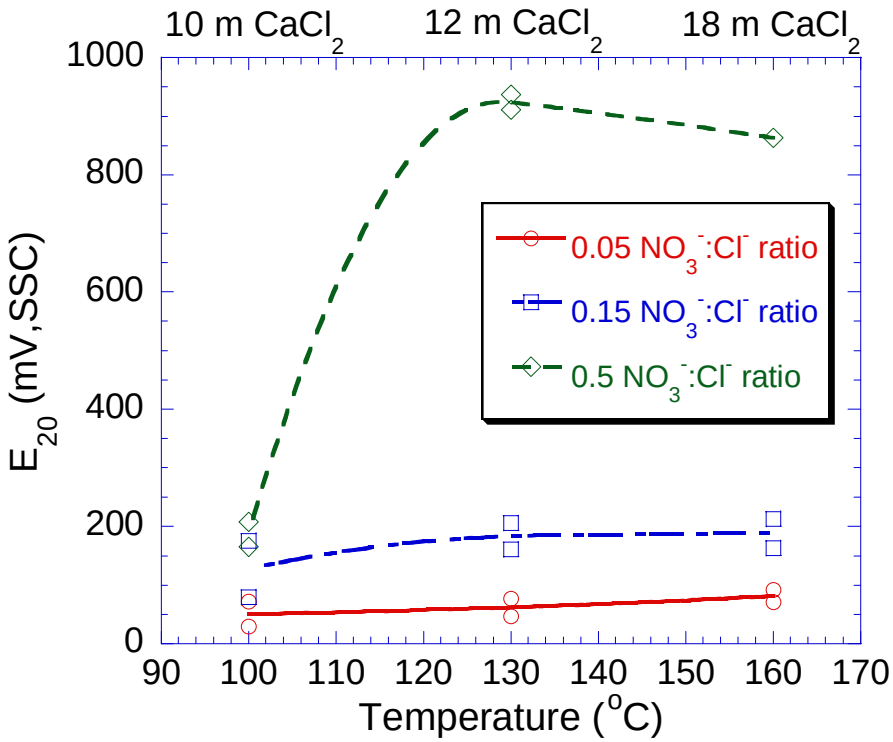

FIGURE 6 - E_{20} values versus temperature (bottom x-axis) and $CaCl_2$ concentration (top x-axis) for 0.05, 0.15 and 0.5 NO_3^-:Cl^- ratios.

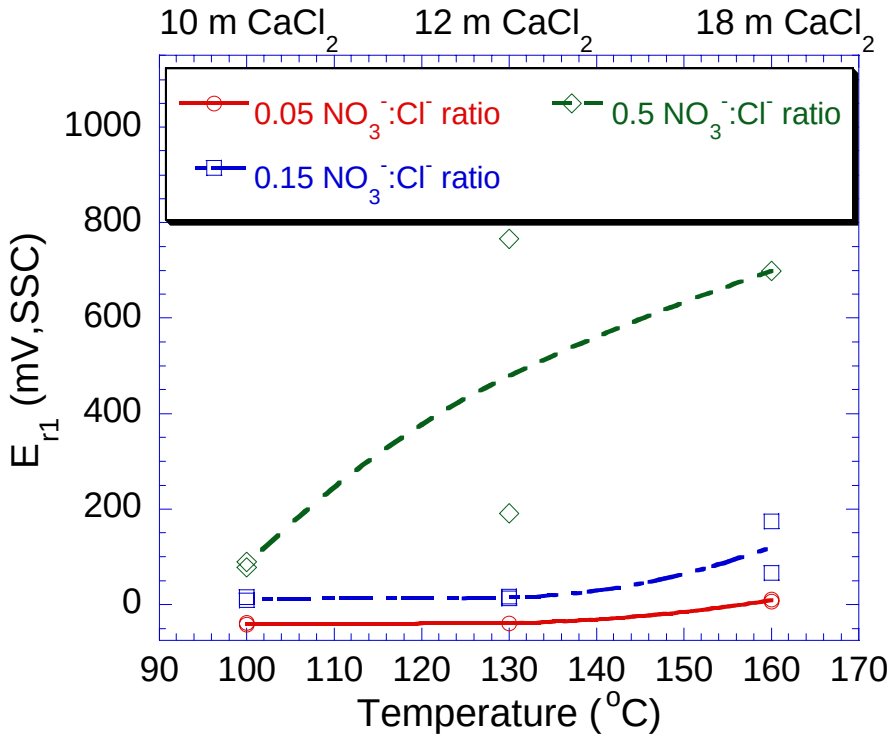

FIGURE 7 - E_{r1} values versus temperature (bottom x-axis) and $CaCl_2$ concentration (top x-axis) for 0.05, 0.15 and 0.5 NO_3^-:Cl^- ratios.

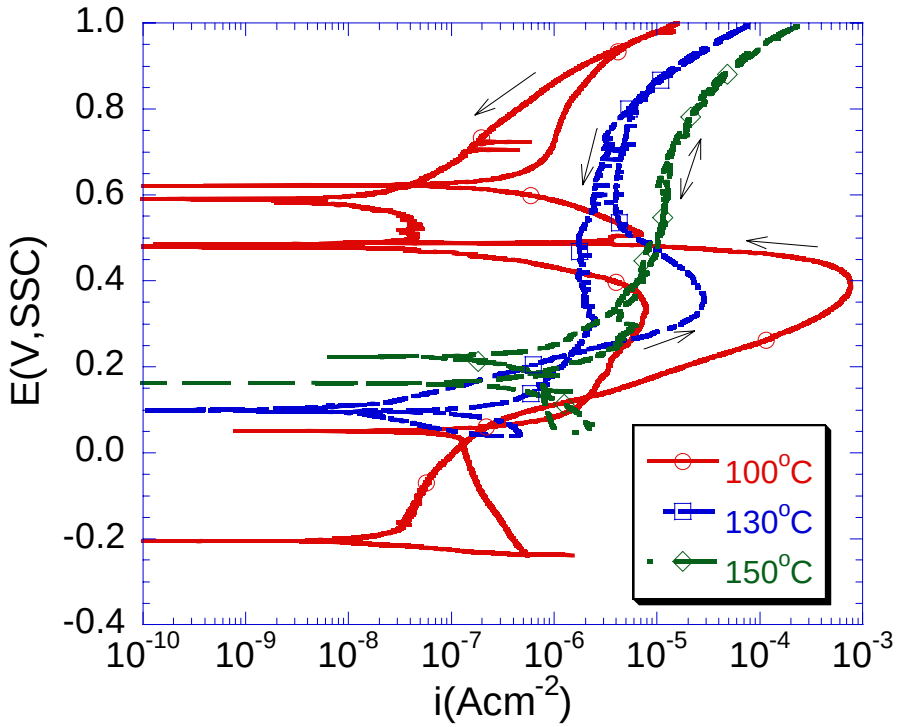

FIGURE 8 - Comparison of polarization curves for 12 molal $CaCl_2$ + 6 molal $Ca(NO_3)_2$ at 100, 130 and 150°C.

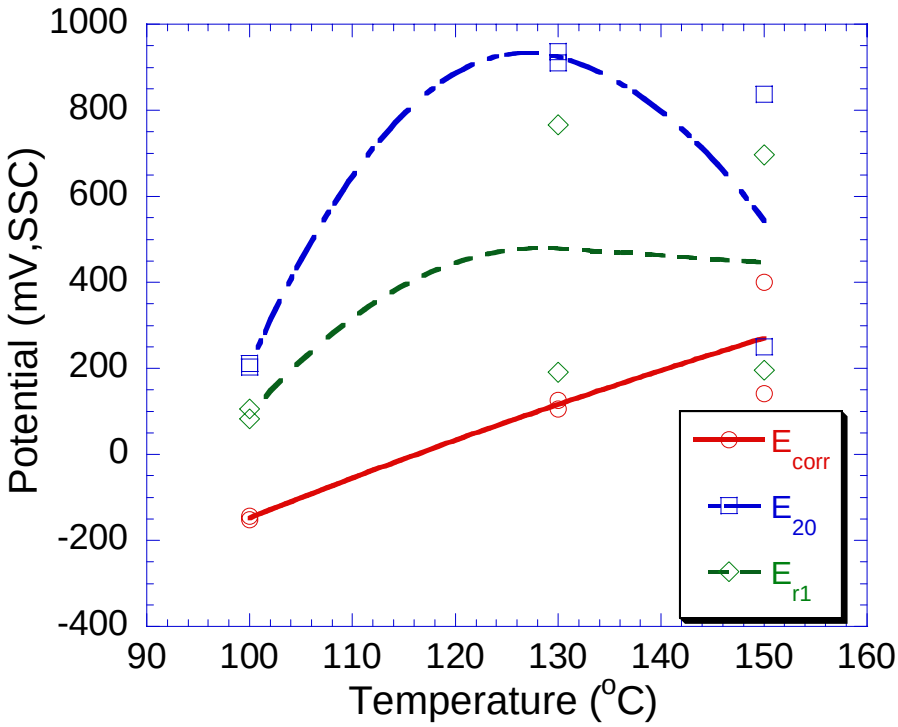

FIGURE 9 - E_{corr}, E_{20} and E_{r1} versus temperature for 12 molal $CaCl_2$ + 6 molal $Ca(NO_3)_2$.

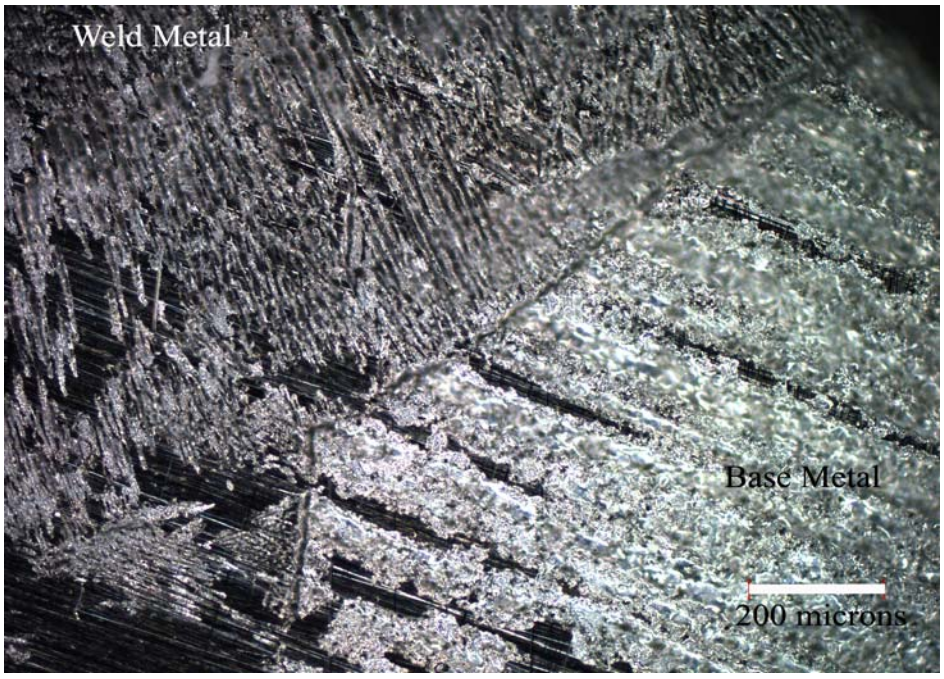

FIGURE 10 - Dark field image of specimen CP tested in 10 m $CaCl_2$ + 1.5 m $Ca(NO_3)_2$ at 100°C. The upper left of the image corresponds to weld metal and the lower right to base metal. Gray and light gray areas are pits.